

An alternative spontaneous symmetry breaking pattern for U(1) with no gapless Goldstone mode

Huan-Qiang Zhou,¹ Qian-Qian Shi,¹ and Yan-Wei Dai¹

¹Centre for Modern Physics, Chongqing University, Chongqing 400044, The People's Republic of China

An emergent gapless Goldstone mode originates from continuous spontaneous symmetry breaking, which has become a doctrine since the pioneering work by Goldstone [J. Goldstone, *Nuovo Cimento* **19**, 154 (1961)]. However, we argue that it is possible for a continuous symmetry group U(1) to make an exceptional case, simply due to the well-known mathematical result that a continuous symmetry group U(1) may be regarded as a limit of a discrete symmetry group Z_q when q tends to infinity. As a consequence, spontaneous symmetry breaking for such a continuous symmetry group U(1) does not necessarily lead to any gapless Goldstone mode. This is explicitly explained for an anisotropic extension of the ferromagnetic spin-1 biquadratic model. In a sense, this model provides an illustrative example regarding the dichotomy between continuity and discreteness.

I. INTRODUCTION

Distinct types of quantum states of matter emerge from spontaneous symmetry breaking (SSB) - a fundamental notion in the conventional Landau-Ginzburg-Wilson paradigm [1]. In particular, if a continuous symmetry group is spontaneously broken, then an emergent gapless Goldstone mode (GM) [2] appears in an attempt to recover the broken symmetry. This is in sharp contrast to SSB for a discrete symmetry group. In a sense, this results in a dichotomy between continuous symmetry groups and discrete symmetry groups, as far as SSB is concerned.

For a relativistic system undergoing SSB, the number of GMs is equal to the number of broken symmetry generators N_{BG} . However, for a non-relativistic system, the connection between the number of GMs and the number of broken symmetry generators N_{BG} is much more involved [3–13]. A proper classification of GMs requires to introduce type-A and type-B GMs [8, 9], as a further development of a previous observation made by Nambu [14]. As a consequence, one is led to the counting rule of GMs that $N_A + 2N_B = N_{BG}$, when the symmetry group G is spontaneously broken into H , where N_A and N_B are, respectively, the numbers of type-A and type-B GMs, and N_{BG} is equal to the dimension of the coset space G/H . In a sense, this classification partially resolves a long-standing debate between Anderson and Peierls concerning whether or not the SU(2) ferromagnetic states originate from SSB [15], given that the SU(2) ferromagnetic states constitute a prototype for SSB from SU(2) to U(1), with the emergence of one type-B GM.

A natural question arises as to whether or not the dichotomy between continuity and discreteness exhausts all the possible types of SSB that occurs, in principle, in quantum many-body systems. Actually, in our opinion, SSB for a symmetry group U(1) occupies a prominent position, since it *only* leads to a type-A GM in two- and higher dimensional quantum many-body systems, if one takes both the Mermin-Wagner-Coleman theorem [16] and the counting rule of GMs [8, 9] into account. As any other patterns for SSB with type-A GMs, it *only* occurs in the thermodynamic limit, in contrast to SSB with type-B GMs. In fact, this SSB pattern is visualized as the Mexican hat in the energy configuration.

Conventionally, SSB is characterized in terms of a singularity arising from the two non-commutative limiting opera-

tions [17]: one is the thermodynamic limit, and the other is to demand that an additional term in the model Hamiltonian, with its density acting as a (local) order parameter and explicitly breaking the symmetry group G , vanishes. However, if $G = U(1)$, the situation becomes quite subtle, due to the fact that U(1) may be regarded as a limit of a cyclic group Z_q , when q tends to infinity. Hence, a SSB pattern for U(1) arises from a singularity due to the non-commutativity of the two limiting operations: one is $L \rightarrow \infty$, and the other is $q \rightarrow \infty$. In fact, such a SSB pattern for U(1) occurs in a superfluid phase, with one type-A GM, in two- and higher dimensions. However, one may imagine an alternative SSB pattern for a continuous symmetry group U(1), if q is simply related with the system size L . In other words, the two limiting operations, i.e., $L \rightarrow \infty$ and $q \rightarrow \infty$, are essentially identical. If so, an alternative SSB pattern for a continuous symmetry group U(1) occurs, with a salient feature that no gapless GM emerges.

In this work, we demonstrate that such an alternative SSB pattern for a continuous symmetry group U(1) does occur in quantum many-body systems, thus leading to an exotic quantum state of matter. As it turns out, the coexisting fractal (CF) phases in the spin-1 ferromagnetic anisotropic biquadratic model offer an illustrative example for this pattern, thus leading to infinitely degenerate (unentangled) factorized ground states that are scale-invariant in the thermodynamic limit, with the fractal dimension d_f , identical to the number of type-B GMs N_B , being zero.

II. THE GROUND STATE PHASE DIAGRAM FOR THE SPIN-1 FERROMAGNETIC ANISOTROPIC BIQUADRATIC MODEL

An anisotropic extension of the spin-1 ferromagnetic biquadratic model [18] is described by the Hamiltonian

$$\mathcal{H} = \sum_j (J_x S_j^x S_{j+1}^x + J_y S_j^y S_{j+1}^y + J_z S_j^z S_{j+1}^z)^2, \quad (1)$$

where S_j^x , S_j^y , and S_j^z are the spin-1 operators at a lattice site j , and J_x , J_y , and J_z denote the coupling parameters describing anisotropic interactions. The sum over j is taken from 1 to $L - 1$ under the open boundary conditions (OBCs) and from 1 to L under the periodic boundary conditions (PBCs).

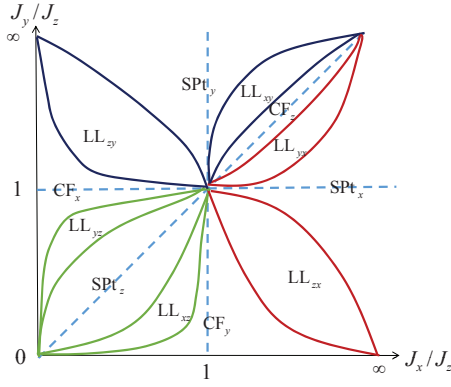


FIG. 1. A sketch of the ground state phase diagram for an anisotropic extension of the spin-1 ferromagnetic biquadratic model (1), which is adapted from Ref. [20] (also cf. Ref.[21]). We focus on the region: $J_x/J_z \geq 0$ and $J_y/J_z \geq 0$, due to a symmetric consideration. Here, a solid line indicates a phase transition line. There are twelve distinct phases: three CF phases labeled as CF_x , CF_y and CF_z , six LL phases labeled as LL_{xy} , LL_{yz} , LL_{zx} , LL_{yx} , LL_{xz} and LL_{zy} , and three SPT phases labeled as SPT_x , SPT_y and SPT_z , respectively. Note that both horizontal and vertical axes are in a scale, defined by $\arctan(J_x/J_z)$ and $\arctan(J_y/J_z)$, respectively.

Its isotropic version is an exactly solvable case in the spin-1 bilinear-biquadratic model [19]. At a generic point in the parameter space, the model Hamiltonian (1) possesses the symmetry group $U(1) \times U(1)$, generated by $K_{yz} \equiv \sum_j K_{yz}^j$ and $K_x \equiv \sum_j K_x^j$, with $K_{yz}^j = \sum_j (-1)^{j+1} [(S_j^y)^2 - (S_j^z)^2]$ and $K_x^j = \sum_j (-1)^{j+1} (S_j^x)^2$, respectively. However, on the three characteristic lines ($J_x = J_y$, $J_y = J_z$ and $J_z = J_x$), the symmetry group is enlarged to $SU(2) \times U(1)$ [20] (for more details, we refer to Sec. A of the Supplemental Material (SM)). The symmetry generators are staggered, thus we have to restrict ourselves to even L 's. The ground state phase diagram is sketched in Fig. 1, which is adapted from Ref. [20] (also cf. Ref. [21]), as a result of the numerical simulation in terms of the iTEBD algorithm [22]. There are twelve distinct phases: three CF phases, labeled as CF_x , CF_y and CF_z , six Luttinger liquid (LL) phases, with central charge $c = 1$, labeled as LL_{xy} , LL_{yz} , LL_{zx} , LL_{yx} , LL_{xz} and LL_{zy} , and three symmetry-protected trivial (SPT) phases [23], labeled as SPT_x , SPT_y and SPT_z , respectively. As demonstrated in Ref. [20], a novel universality class arises from instabilities of the LL phases towards the CF phases. In addition, QPTs between the LL phases and the SPT phases are identified to be in the KT universality class.

Before proceeding, we remark that the three CF phases, six LL phases and three SPT phases are dual to each other under duality transformations induced from the permutation group S_3 with respect to S_j^x , S_j^y and S_j^z : $S_j^x \leftrightarrow S_j^y$, $S_j^y \leftrightarrow S_j^z$ and $S_j^z \leftrightarrow S_j^x$ [20]. Hence, we restrict ourselves to characterize the CF_x phase, the LL_{yz} phase, and the SPT_z phase.

We start with the two characteristic lines $J_y/J_z = 1$ and $J_x = 0$, located inside the CF_x phase. On the characteristic line $J_y/J_z = 1$, highly degenerate ground states occur, with the ground state energy per lattice site being equal to J_x^2 and the ground state degeneracy being $L + 1$, as a result of SSB

from $SU(2) \times U(1)$ to $U(1) \times U(1)$ [20, 24, 25], with one type-B GM [20]. Hence, the highly degenerate ground states are scale-invariant, characterized in terms of the fractal dimension d_f [26] (also cf. Ref. [27]). As argued in Refs. [20, 25], the entanglement entropy exhibits a logarithmic scaling relation with the block size N in the thermodynamic limit $L \rightarrow \infty$, with the prefactor being half the number of type-B GMs N_B , thus leading to the identification of the fractal dimension d_f with the number of type-B GMs N_B . We remark that both the highest and lowest weight states are (unentangled) factorized states, with the entanglement entropy being zero.

Now we turn to the characteristic line $J_x = 0$ with $J_y/J_z > 0$ in the CF_x phase. On this characteristic line, there are a two-parameter family of factorized ground states $|\phi_f\rangle$, with the ground state degeneracy being $L + 1$, and the ground state energy per lattice site being equal to 0. The explicit expression for $|\phi_f\rangle$ has been presented in Ref. [20] (also cf. Sec. A of the SM). Instead, we are interested in a particular factorized ground state $|\phi_0\rangle = \bigotimes_j |v\rangle_j$, where $|v\rangle_j = \mu|0_y\rangle_j + \nu|0_z\rangle_j$, with $\mu^2 + \nu^2 = 1$ and $\mu = \sqrt{J_y/(J_y + J_z)}$. Here, $|0_y\rangle_j$ and $|0_z\rangle_j$ are basis states, with an eigenvalue being zero, for the spin operators S_j^y and S_j^z , respectively. Actually, a two-parameter family of factorized ground states $|\phi_f\rangle$ are generated from the action of the symmetry group $U(1) \times U(1)$ on $|\phi_0\rangle$. Note that the ground state $|\phi_0\rangle$ is invariant under the one-site translation operation if PBCs are adopted or under the permutation $P_{12}P_{23} \cdots P_{L-1,L}$ if OBCs are adopted, where P_{kk+1} ($k = 1, \dots, L-1$) denote the generators of the permutation group S_L . Moreover, $|\phi_0\rangle$ evolves into the highest weight state $|\otimes_{j=1}^L \{1_x\}_j\rangle$ for the symmetry group $SU(2)$, as J_y tends to J_z . Here, $|1_x\rangle$ denotes the eigenvector of S_j^x , with the eigenvalues being 1.

It is convenient to introduce q H-orthogonal states $|\psi_k\rangle$ ($k = 0, 1, \dots, L$), defined as $|\psi_k\rangle \equiv (V_q)^k |\phi_0\rangle$, where V_q denotes an operator $V_q = \prod_j \exp(i2\pi K_{yz}^j/q)$, with $q = L + 1$. Indeed, V_q itself is an element of a cyclic group Z_q , which turns out to be a subgroup of the symmetry group $U(1)$ generated by K_{yz} . Here, we mention that the notion of q -orthogonal states has been introduced to describe SSB for discrete symmetry groups in Ref. [28]. Hence, it is the cyclic group Z_q that connects the q -orthogonal states $|\psi_k\rangle$, which becomes $U(1)$ in the thermodynamic limit. As a result, an alternative SSB pattern for a continuous symmetry group $U(1)$ occurs on the characteristic line $J_x = 0$ with $J_y/J_z > 0$, with a salient feature that no gapless GM emerges.

A remarkable fact is that the highly degenerate ground states are permutation-invariant with respect to the unit cells consisting of the two nearest-neighbor lattice sites on the two characteristic lines $J_y/J_z = 1$ and $J_x = 0$. That is, there is an *emergent* permutation symmetry group $S_{L/2}$ in the ground state subspace, given the Hamiltonian 1 is not permutation-invariant. In fact, the CF_x phases may be attributed to the coexistence of $SU(2)$ SSB with one type-B GM [7–9] on the characteristic line $J_y/J_z = 1$ and an alternative SSB pattern for $U(1)$ without any gapless GM on the characteristic line $J_x = 0$ with $J_y/J_z > 0$.

III. THE GROUND STATE AND THE LOW-LYING STATES

We aim to reveal distinct features for the three phases - the CF_x phase, the LL_{yz} phase, and the SPT_z phase, by performing numerical simulations in terms of the exact diagonalization (ED). For a chosen value of the system size L , we focus on the ground state $|\varphi_0\rangle$ and (up to L) low-lying states, labeled as $|\varphi_k\rangle$, with $k = 1, \dots, L$.

In the SPT_z phase, we evaluate the ground state $|\varphi_0\rangle$ and a few (up to L) low-lying states $|\varphi_k\rangle$, together with their eigenvalues E_k ($k = 0, 1, \dots, L$). There is only a unique ground state, and the other low-lying states do not exhibit any pattern (for more details, cf. Sec. B of the SM). Further, we evaluate the entanglement entropy $S(L, N)$, as a function of the block size N , for the point $(J_x/J_z, J_y/J_z) = (0.2, 0.3)$ in the SPT_z phase. It is found that the entanglement entropy $S(L, N)$ saturates, as the block size n increases. Thus, the SPT_z phase is gapped (for more details, cf. Sec. C of the SM).

In the LL_{yz} phase, we evaluate the ground state $|\varphi_0\rangle$ and L low-lying states $|\varphi_k\rangle$ ($k = 1, \dots, L$) for a few chosen values of L , together with their eigenvalues E_k ($k = 0, 1, \dots, L$). It is found that the l -th and $L + 1 - l$ -th low-lying states, i.e., $|\varphi_l\rangle$ and $|\varphi_{L+1-l}\rangle$, are degenerate in pair, with the energy eigenvalues $E_l = E_{L+1-l}$ ($l = 1, \dots, L/2$), where l ranges from 1 to $L/2$, in addition to the non-degenerate ground state $|\varphi_0\rangle$. The energy gap $\Delta_{0L/2}(L)$ between the ground state $|\varphi_0\rangle$ and the $L/2$ -th low-lying state $|\varphi_{L/2}\rangle$, denoted as $\Delta_{0L/2}(L)$, scales as $\Delta_{0L/2}(L) \sim L$, thus indicating that the ratio $\Delta_{0L/2}(L)/L$ survives, as L increases, in the LL_{yz} phase (for more details, cf. Sec. B of the SM). In order to lend further support for the fact that the LL_{yz} phase is a LL phase, the finite-size matrix product state (MPS) algorithm [29] has been exploited to extract central charge c . In fact, a finite-size scaling analysis of the entanglement entropy yields $c = 1$ [20] (for more details, cf. Sec. C of the SM).

In the CF_x phase, we evaluate the ground state $|\varphi_0\rangle$ and L low-lying states $|\varphi_k\rangle$ ($k = 1, \dots, L$) for a few chosen values of L , together with their eigenvalues E_k ($k = 0, 1, \dots, L$). It is found that the l -th and $L + 1 - l$ -th low-lying states, i.e., $|\varphi_l\rangle$ and $|\varphi_{L+1-l}\rangle$, are degenerate in pair, with the energy eigenvalues $E_l = E_{L+1-l}$ ($l = 1, \dots, L/2$), where l ranges from 1 to $L/2$, in addition to the non-degenerate ground state $|\varphi_0\rangle$. This pattern is exactly identical to that in the LL_{yz} phase. However, the energy gap between the ground state $|\varphi_0\rangle$ and the $L/2$ -th low-lying state $|\varphi_{L/2}\rangle$, denoted as $\Delta_{0L/2}(L)$, scales in a drastically different way, and the ratio $\Delta_{0L/2}(L)/L$ vanishes in the thermodynamic limit $L \rightarrow \infty$ (for more details, cf. Sec. B of the SM).

We remark that, in both the LL_{yz} phase and the CF_x phase, $|\varphi_k\rangle$ ($k = 0, 1, \dots, L$) are simultaneous eigenvectors of the model Hamiltonian (1) and V_q . More precisely, we have $H|\varphi_k\rangle = E_k|\varphi_k\rangle$ and $V_q|\varphi_k\rangle = \exp(i2\pi k/q)|\varphi_k\rangle$ ($k = 0, 1, \dots, L$). In this sense, $|\varphi_k\rangle$ ($k = 0, 1, \dots, L$) constitute a one-dimensional representation for the cyclic group Z_q . In the thermodynamic limit $L \rightarrow \infty$, Z_q becomes the symmetry group $U(1)$ generated by K_{yz} . In addition, $|\varphi_k\rangle$ ($k = 0, 1, \dots, L$) are always invariant under the symmetry group $U(1)$ generated by K_x .

Apart from the commonalities for the LL_{yz} phase and the CF_x phase, we are more interested in the differences between them. The emergence of the cyclic group Z_q is one of the characteristic features in both the LL_{yz} phase and the CF_x phase. Actually, the $L/2$ -th and $L/2 + 1$ -th low-lying states, which form the pair with the energy eigenvalue $J_x^2 L$, take the form $|\otimes_l \{0_y\}0_z\}_l\rangle$ and $|\otimes_l \{0_z\}0_y\}_l\rangle$, respectively, in the two phases. However, the gap $\Delta_{0L/2}$ survives in the LL_{yz} phase, but vanishes in the CF_x phase, when the thermodynamic limit is approached. This observation makes it possible to distinguish the CF phases from the LL phases.

The essential difference manifests itself in the observation that the ground state $|\varphi_0\rangle$ and L low-lying states $|\varphi_k\rangle$ ($k = 1, \dots, L$) are quasi-degenerate in the CF_x phase, but not in the LL_{yz} phase. The consequence will be elaborated on in the context of H-orthogonal states [28] below. Physically, the H-orthogonal states offer a description for a finite-size precursor to the $U(1)$ symmetry-broken states that *only* occur in the thermodynamic limit, thus leading to an alternative SSB pattern for $U(1)$ in the CF_x phase. In contrast, this is not true for $|\varphi_k\rangle$ ($k = 0, 1, \dots, L$) in the LL_{yz} phase, given that the low energy physics is described as a conformal field theory.

Meanwhile, given a permutation symmetry group $S_{L/2}$ for the ground state subspace emerges on the two characteristic lines $J_y/J_z = 1$ and $J_x = 0$ and they are located in the CF_x phase, one may anticipate that there exists an emergent permutation symmetry group $S_{L/2}$, away from the two characteristic lines $J_y/J_z = 1$ and $J_x = 0$. As it turns out, such an emergent permutation symmetry group $S_{L/2}$ for the ground state subspace is approximate for finite L 's, but becomes exact when L tends to infinity (for more details, cf. Sec. D of the SM).

IV. H-ORTHOGONALITY AND AN ALTERNATIVE SSB PATTERN FOR $U(1)$

Given we are able to construct exactly the q H-orthogonal states on the characteristic line $J_x = 0$, it is plausible to resort to a generic scheme on H-orthogonal states [28] to characterize an alternative SSB pattern for $U(1)$ in the CF_x phase, away from the two characteristic lines $J_y/J_z = 1$ and $J_x = 0$. As a result of the cyclic group Z_q , the Hilbert space is separated into disjoint sectors, labeled by the phases $w_k = \exp(i2\pi k/q)$, with $k = 0, 1, 2, \dots, q-1$, as far as the low-energy physics is concerned. More precisely, we construct q H-orthogonal states $|\psi_k\rangle$ from the ground state $|\varphi_0\rangle$ and the low-lying states $|\varphi_k\rangle$ ($k = 1, \dots, L$):

$$|\psi_k\rangle = \sum_{k'=0}^{q-1} c_{k'}(w_k)^{k'} |\varphi_{k'}\rangle. \quad (2)$$

Here, $|\psi_k\rangle$ is normalized so that $\sum_k |c_k|^2 = 1$. However, they are not orthogonal to each other. Instead, $|\psi_k\rangle$ ($k = 0, 1, 2, \dots, q-1$) satisfy the H-orthogonality [28]

$$\langle \psi_k' | H | \psi_k \rangle = 0, \text{ if } k \neq k'.$$

Then we have

$$\begin{aligned} |c_k|^2 E_k &= |c_{q-1}|^2 E_{q-1}, \\ |c_{q-1}|^2 E_{q-1} &= \frac{1}{\sum_{k=0}^{q-1} \frac{1}{E_k}}. \end{aligned} \quad (3)$$

From $E_l = E_{q-l}$ ($l = 1, \dots, L/2$), it follows that $|c_l|^2 = |c_{q-l}|^2$. In fact, the low-lying state $|\varphi_l\rangle$ is mapped to the low-lying state $|\varphi_{q-l}\rangle$ and vice versa under the one-site translation operation if PBCs are adopted or under the permutation $P_{12}P_{23}\dots, P_{L-1,L}$ if OBCs are adopted. In particular, the ground state is invariant under the one-site translation operation if PBCs are adopted or under the permutation $P_{12}P_{23}\dots, P_{L-1,L}$ if OBCs are adopted. We stress that the one-site translation operation is a symmetry operation under PBCs. However, it does not commute with the generators K_{yz} and K_x of the symmetry group $U(1) \times U(1)$. Hence, it is impossible to simultaneously diagonalize the model Hamiltonian (1), the generators K_{yz} and K_x of the symmetry group $U(1) \times U(1)$ and the one-site translation operation under PBCs. Here, we have chosen to simultaneously diagonalize the model Hamiltonian (1) and the generators K_{yz} and K_x of the symmetry group $U(1) \times U(1)$.

A peculiar feature of the q H-orthogonal states $|\psi_k\rangle$ ($k = 0, 1, 2, \dots, L$) is that they satisfy a cyclic relation: $|\psi_{k+1}\rangle = V_q|\psi_k\rangle$. This cyclic relation implies that the fidelity $\langle\psi_{k'}|\psi_k\rangle$ between any two H-orthogonal states $|\psi_{k'}\rangle$ and $|\psi_k\rangle$ scales with the system size L exponentially, i.e., $\langle\psi_{k'}|\psi_k\rangle \equiv d_{kk'}^L$, with $d_{kk'}$ being the fidelity per lattice site [30], which vanishes in the thermodynamic limit, if $k \neq k'$. Physically, the H-orthogonal states may be understood as a finite-size precursor to the symmetry-broken states arising from an alternative SSB pattern for $U(1)$ that *only* occurs in the thermodynamic limit. However, it is necessary to require that the ground state $|\varphi_0\rangle$ and L low-lying states $|\varphi_k\rangle$ ($k = 1, \dots, L$) are quasi-degenerate, in order to ensure the existence of the H-orthogonal states.

Conversely, the ground state $|\varphi_0\rangle$ and the low-lying states $|\varphi_k\rangle$ ($k = 1, \dots, L$) may be expressed in terms of the q H-orthogonal states $|\psi_k\rangle$

$$|\varphi_k\rangle = \frac{1}{c_k} \sum_{k'=0}^{q-1} (w_{k'})^{-k} |\psi_{k'}\rangle. \quad (4)$$

Note that the energy expectation value \bar{E}_k for a H-orthogonal state, defined as $\langle\psi_k|\mathcal{H}|\psi_k\rangle$, is identical for any k : $\bar{E}(L)_k = \bar{E}(L)$. In fact, $\bar{E}(L)$ takes the form

$$\bar{E}(L) = \sum_{k=0}^L |c_k(L)|^2 E_k(L) = E_0(L) + \sum_{k=1}^L |c_k(L)|^2 \Delta_k(L), \quad (5)$$

with $\Delta_k(L) = (E_k(L) - E_0(L))$ being the k -th energy gap. Note that $\sum_{k=1}^L |c_k(L)|^2 \Delta_k(L) = 2 \sum_{l=1}^{L/2} |c_l(L)|^2 \Delta_l(L)$. If one expresses $|c_l(L)|^2$ in terms of $\langle\psi_{k'}|\psi_k\rangle$, then $\sum_{l=1}^{L/2} |c_l(L)|^2 \Delta_l(L)$ is split into two parts: $\sum_{l=1}^{L/2} |c_l(L)|^2 \Delta_l(L) = 1/q \sum_{l=1}^{L/2} \Delta_l(L) + \sum_{l=1}^{L/2} (|c_l(L)|^2 - 1/q) \Delta_l(L)$. Here, $1/q \sum_{l=1}^{L/2} \Delta_l(L) \approx 1/L \sum_{l=1}^{L/2} \Delta_l(L)$ is half the arithmetic average $\Delta_a(L)$ of the gaps

$\Delta_k(L) = (E_k(L) - E_0(L))$. For fixed L , $|c_l(L)|^2$ decreases and $\Delta_l(L)$ increases, as l increases from 1 to $L/2$. Hence, $(|c_l(L)|^2 - 1/q) \Delta_l(L)$ is smoothly varying as l increases. Taking into account the fact that the fidelity between any two H-orthogonal states scales with the system size L exponentially, and combining with an observation that both $|c_k(L)|^2$ and $\Delta_k(L)$, as a function of L , are monotonically decreasing with increasing L , we neglect $\sum_{l=1}^{L/2} (|c_l(L)|^2 - 1/q) \Delta_l(L)$, or equivalently, $\sum_{k=1}^L (|c_k(L)|^2 - 1/q) \Delta_k(L)$, and make a reasonable estimate $\Delta_a(L) \approx BL \exp(-\kappa L)$, with B and κ being positive constants. Hence, the ground state energy E_0 becomes

$$E_0(L) \approx \bar{E}(L) - B L e^{-\kappa L}. \quad (6)$$

We are led to conclude that, for a finite system size L , the ground state $|\varphi_0\rangle$ and the low-lying states $|\varphi_k\rangle$ ($k = 1, \dots, L$) in the CF_x phase are quasi-degenerate, due to the presence of q H-orthogonal states $|\psi_k\rangle$, in sharp contrast to their counterparts in the LL_{yz} phase. We remark that the CF_x phase becomes infinitely degenerate in the thermodynamic limit $L \rightarrow \infty$, as a result of an alternative SSB pattern for $U(1)$, featuring that no gapless GM emerges. This is due to the fact that this SSB pattern for a continuous symmetry group $U(1)$ is *only* a limit of a SSS pattern for a discrete symmetry group Z_q , when q tends to infinity. Indeed, infinitely degenerate ground states are (unentangled) factorized states so that they are scale-invariant. Actually, one may still introduce the fractal dimension d_f to describe scale-invariant factorized states, with d_f being zero [21]. In fact, the number of type-B GMs N_B , identical to the fractal dimension d_f , must be zero, as follows from the counting rule of GMS [8, 9], given only one generator K_{yz} is broken.

As a result of this SSB pattern for $U(1)$, infinitely degenerate ground states, as (unentangled) factorized states, are permutation-invariant. Hence, the emergent permutation symmetry $S_{L/2}$ (with respect to the unit cells consisting of the two nearest-neighbor lattice sites) in the ground state subspace, as already observed on the two characteristic lines $J_y/J_z = 1$ and $J_x = 0$, exist in the entire CF_x phase, when the thermodynamic limit is approached.

V. FINITE-SIZE CORRECTIONS TO THE GROUND STATE ENERGY E_0 : EMERGENT PERMUTATION SYMMETRY

An asymptotic analysis, up to the first-order correction, is performed for the q H-orthogonal states $|\psi_k\rangle$ in Sec. E of the SM. As a result, the energy expectation value \bar{E}_k for a H-orthogonal state takes the form

$$\bar{E}(L) = J_x^2 L - A e^{\eta/L}, \quad (7)$$

where $A = 2a^2/\omega_0$ and $\eta = \omega_0 g/(2a^2)$, with g being a positive constant, and $a = J_x(J_z - J_y)$. Hence, the ground state energy $E_0(L)$ takes the form

$$E_0(L) = J_x^2 L - A e^{\eta/L} - B L e^{-\kappa L}. \quad (8)$$

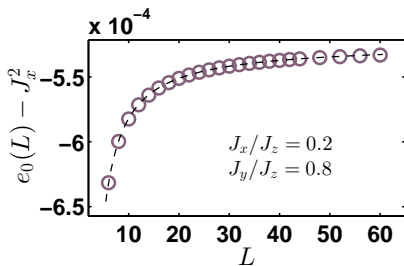


FIG. 2. (color online) The finite-size corrections to the ground state energy per lattice site, denoted as $e_0(L)$, for the point (0.2, 0.8) in the CF_x phase. Here, the finite-size DMRG algorithm is exploited to simulate the model (1) under PBCs, with the system size L ranging from 6 to 60. The best fit yields that $A = 4.735 \times 10^{-4}$, $B = 5.255 \times 10^{-4}$, $\eta = 1.8$, and $\kappa = 0.2687 \times 10^{-4}$ in Eq.(8).

Physically, two length scales are competing with each other in the CF_x phase: one is involved in the second term originating from the emergent permutation symmetry in the ground state subspace and the other is involved in the third term, originating from an alternative SSB pattern for $U(1)$.

For a few randomly chosen points in the CF_x phase, it is found that the ground state energy $E_0(L)$, evaluated from the finite-size density matrix renormalization group (DMRG) simulations [31], agrees well with the theoretical prediction in Eq. 8, even for small L 's, with L ranging from 6 to 60, as seen in Fig. 2 from our simulation results for the point (0.2, 0.8) in the CF_x phase (for more details, cf. Sec. F of the SM). This lends further support to our conclusion that the CF_x phase results from an alternative SSB pattern for the symmetry group $U(1)$ generated from K_{yz} , thus leading to infinitely degenerate ground states that are scale-invariant in the thermodynamic limit, thus representing an exotic quantum state of matter.

The finite-size corrections to the ground state energy mark an essential difference between the CF_x phase and the LL_{yz} phase. The former is scale-invariant, but not conformally invariant, whereas the latter is conformally invariant, with central charge $c = 1$, subject to the finite-size corrections to

the ground state energy predicted from conformal field theory [32].

VI. SUMMARY

A systematic investigation has been carried out for an anisotropic extension of the ferromagnetic spin-1 biquadratic model, in an attempt to characterize the three distinct types of phases - the SPT phases, the LL phases, and the CF phases. As it turns out, the SPT phases are gapped, whereas the LL phases are gapless and conformally invariant. In contrast, the CF phases represent an exotic quantum state of matter, which results from an alternative SSB pattern for $U(1)$, with a salient feature that no gapless GM emerges. Meanwhile, such an alternative SSB pattern for $U(1)$ yields infinitely degenerate ground states in the thermodynamic limit, which turn out to be (unentangled) factorized states. Hence, they are scale-invariant, with the fractal dimension d_f , identical to the number of type-B GMs N_B , being zero [21].

In conclusion, the presence of an alternative SSB pattern for $U(1)$ does not challenge the counting rule of GMs for continuous SSB, since no GM emerges. However, it does require clarification of the semantic meaning for continuous SSB in the Goldstone theorem [2], since $U(1)$, as a continuous symmetry group, makes an exceptional case, simply due to the well-known mathematical result that a continuous symmetry group $U(1)$ may be regarded as a limit of a discrete symmetry group Z_q , when q tends to infinity. That is, the dichotomy between continuity and discreteness is more involved than one might have expected.

VII. ACKNOWLEDGEMENTS

We are grateful to Murray Batchelor, John Fjaerestad and Ian McCulloch for comments and suggestions to improve the manuscript.

-
- [1] P. W. Anderson, Basic Notions of Condensed Matter Physics, Addison-Wesley: The Advanced Book Program (Addison-Wesley, Reading, MA, 1997).
 - [2] J. Goldstone, Nuovo Cimento **19**, 154 (1961); J. Goldstone, A. Salam, and S. Weinberg, Phys. Rev. **127**, 965 (1962); Y. Nambu and G. Jona-Lasinio, Phys. Rev. **122**, 345 (1961).
 - [3] H. B. Nielsen and S. Chadha, Nucl. Phys. B **105**, 445 (1976).
 - [4] T. Schäfer, D. T. Son, M. A. Stephanov, D. Toublan, and J. J. M. Verbaarschot, Phys. Lett. B **522**, 67 (2001).
 - [5] V. A. Miransky and I. A. Shovkovy, Phys. Rev. Lett. **88**, 111601 (2002).
 - [6] A. Nicolis and F. Piazza, Phys. Rev. Lett. **110**, 011602 (2013).
 - [7] H. Watanabe and T. Brauner, Phys. Rev. D **84**, 125013 (2011).
 - [8] H. Watanabe and H. Murayama, Phys. Rev. Lett. **108**, 251602 (2012).
 - [9] H. Watanabe and H. Murayama, Phys. Rev. X **4**, 031057 (2014).
 - [10] Y. Hidaka, Phys. Rev. Lett. **110**, 091601 (2013).
 - [11] H. Watanabe, T. Brauner, and H. Murayama, Phys. Rev. Lett. **111**, 021601 (2013).
 - [12] T. Hayata and Y. Hidaka, Phys. Rev. D **91**, 056006 (2015).
 - [13] D. A. Takahashi and M. Nitta, Ann. Phys. **354**, 101 (2015).
 - [14] Y. Nambu, J. Stat. Phys. **115**, 7 (2004).
 - [15] P. W. Anderson, Phys. Today **43**, 5, 117 (1990); R. Peierls, Phys. Today, **44**, 2, 13 (1991).
 - [16] N. D. Mermin and H. Wagner, Phys. Rev. Lett. **17**, 1133 (1966); S. R. Coleman, Commun. Math. Phys. **31**, 259 (1973).
 - [17] M. Berry, Phys. Today **55**, 10 (2002).
 - [18] M. N. Barber and M. T. Batchelor, Phys. Rev. B **40**, 4621 (1989); A. Klümper, Europhys. Lett. **9**, 815 (1989).
 - [19] A. V. Chubukov, Phys. Rev. B **43**, 3337 (1991); G. Fáth and J. Sólyom, Phys. Rev. B **51**, 3620 (1995).
 - [20] Q.-Q. Shi, Y.-W. Dai, S.-H. Li, and H.-Q. Zhou, arXiv: 2204.05692(2022).

- [21] H.-Q. Zhou, Q.-Q. Shi, and Y.-W. Dai, *Entropy*, **24**, 1306 (2022).
- [22] G. Vidal, *Phys. Rev. Lett.* **91**, 147902 (2003); G. Vidal, *Phys. Rev. Lett.* **93**, 040502 (2004); G. Vidal, *Phys. Rev. Lett.* **98**, 070201 (2007).
- [23] Y. Fuji, F. Pollmann, and M. Oshikawa, *Phys. Rev. Lett.* **114**, 177204 (2015). X.-H. Chen, I. P. McCulloch, M. T. Batchelor, and H.-Q. Zhou, *Phys. Rev. B* **102**, 085146 (2020).
- [24] Q.-Q. Shi, Y.-W. Dai, H.-Q. Zhou, and I. P. McCulloch, arXiv: 2201.01071 (2022).
- [25] Q.-Q. Shi, Y.-W. Dai, H.-Q. Zhou, and I. P. McCulloch, arXiv: 2201.01071 (2022).
- [26] O. A. Castro-Alvaredo and B. Doyon, *J. Stat. Mech.*, 2011: P02001 (2011); O. A. Castro-Alvaredo and B. Doyon, *Phys. Rev. Lett.* **108**, 120401 (2012).
- [27] V. Popkov and M. Salerno, *Phys. Rev. A* **71**, 012301 (2005); V. Popkov, M. Salerno, and G. Schütz, *Phys. Rev. A* **72**, 032327 (2005).
- [28] Q.-Q. Shi, H.-Q. Zhou, and M. T. Batchelor, *Sci. Rep.* **5**, 7673 (2015).
- [29] F. Verstraete, D. Porras, and J. I. Cirac, *Phys. Rev. Lett.* **93**, 227205 (2004).
- [30] H.-Q. Zhou and J. P. Barjaktarevic, *J. Phys. A Math. Theor.* **41**, 412001 (2008); H.-Q. Zhou, R. Orús, and G. Vidal, *Phys. Rev. Lett.* **100**, 080601 (2008).
- [31] S. R. White, *Phys. Rev. Lett.* **69**, 2863 (1992); S. R. White, *Phys. Rev. B*, **48**, 345 (1993).
- [32] H. W. J. Blöte, J. Cardy, and M. P. Nightingale, *Phys. Rev. Lett.* **56** 742 (1986); I. Affleck, *Phys. Rev. Lett.* **56**, 746 (1986).

SUPPLEMENTARY MATERIAL

A. Some exact results on the two characteristic lines: $J_y/J_z = 1$ and $J_x/J_z = 0$

For our purpose, we present some exact results in details on the two characteristic lines: $J_y/J_z = 1$ with $J_x/J_z < 1$ and $J_x/J_z = 0$ with $J_y/J_z > 0$.

On the characteristic line: $J_y/J_z = 1$ with $J_x/J_z < 1$, there is one symmetry group $SU(2)$, generated by $\Sigma_x = \sum_j (-1)^{j+1} (S_j^y S_j^z + S_j^z S_j^y)/2$, $\Sigma_y = \sum_j S_j^x/2$, and $\Sigma_z = K_{yz}/2$, together with one symmetry group $U(1)$, generated by $K_x = \sum_j (-1)^{j+1} (S_j^x)^2$. A SSB pattern from $SU(2) \times U(1)$ to $U(1) \times U(1)$ arises, thus leading to highly degenerate ground states, with the ground state energy E_0 being equal to $J_x^2 L$. Two of the degenerate ground states are invariant under the one-site translation operation: $|\otimes_{j=1}^L \{1_x\}_j\rangle$ and $|\otimes_{j=1}^L \{-1_x\}_j\rangle$, where $|1_x\rangle$ and $|-1_x\rangle$ are the eigenvectors of S_j^x , with the eigenvalues being 1 and -1 , respectively. Actually, $|\otimes_{j=1}^L \{1_x\}_j\rangle$ and $|\otimes_{j=1}^L \{-1_x\}_j\rangle$ are the highest and lowest weight states for the symmetry group $SU(2)$ in the Σ_y representation. Indeed, a sequence of degenerate ground states $|L, M\rangle_y$ are generated from the repeated action of the lowering operator Σ_- of the symmetry group $SU(2)$ in the Σ_y representation on the highest weight state $|\otimes_{j=1}^L \{1_x\}_j\rangle$: $|L, M\rangle_y = 1/\sqrt{C_L^M \Xi_-^M} |\otimes_{j=1}^L \{1_x\}_j\rangle$. Meanwhile, $|\otimes_{j=1}^{L/2} \{0_z 0_y\}_j\rangle$ and $|\otimes_{j=1}^{L/2} \{0_y 0_z\}_j\rangle$ are the highest and lowest weight states for the symmetry group $SU(2)$ in the Σ_z representation. Therefore, a sequence of degenerate ground state $|L, M\rangle_z$ generated from the repeated action of the lowering operator Σ_- of the symmetry group $SU(2)$ in the Σ_z representation on the highest weight state $|\otimes_{j=1}^{L/2} \{0_z 0_y\}_j\rangle$: $|L, M\rangle_z \equiv \frac{1}{\sqrt{C_L^M}} \Sigma_-^M |\otimes_{j=1}^{L/2} \{0_z 0_y\}_j\rangle$. As shown in Refs. [S1, S2], the entanglement entropy $S(L, N)$ for this type of degenerate ground states arising from SSB with type-B GMs exhibits a logarithmic scaling relation with the block size N in the thermodynamic limit $L \rightarrow \infty$, with the prefactor being half the number of type-B GMs N_B : $N_B = 1$, as long as the filling $f \equiv M/L$ is non-zero.

On the characteristic line $J_x/J_z = 0$ with $J_y/J_z > 0$, there exists a two-parameter family of factorized ground states $|\phi_f(L)\rangle = \otimes_l |v_1 v_2\rangle_l$ [S3], where $|v_1 v_2\rangle_l = |v_1\rangle_{2l-1} |v_2\rangle_{2l}$, with $|v_1\rangle_{2l-1}$ and $|v_2\rangle_{2l}$ being given in Eq. (S6). The number of linearly independent ground states is $q = L + 1$. We remark that there are *only* two factorized ground states $|\phi_0\rangle$ and $|\phi_{a0}\rangle$, invariant under the one-site translation operation: one is $|\phi_0\rangle = \otimes_j |v\rangle_j$, where $|v\rangle_j = \mu |0_y\rangle_j + \nu |0_z\rangle_j$, with $\mu = \sqrt{J_y/(J_y + J_z)}$ and $\nu = \sqrt{J_z/(J_y + J_z)}$, and the other is $|\phi_{a0}\rangle = \otimes_j |v\rangle_j$, where $|v\rangle_j = \mu |0_y\rangle_j + \nu |0_z\rangle_j$, with $\mu = \sqrt{J_y/(J_y + J_z)}$ and $\nu = -\sqrt{J_z/(J_y + J_z)}$. Note that $|\phi_0\rangle$ and $|\phi_{a0}\rangle$ evolve into $|\otimes_{j=1}^L \{1_x\}_j\rangle$ and $|\otimes_{j=1}^L \{-1_x\}_j\rangle$, as J_y tends to J_z . From both $|\phi_0\rangle$ and $|\phi_{a0}\rangle$, we may construct two sequences of the q H-orthogonal states: $|\psi_k\rangle \equiv V_q^k |\phi_0\rangle$ and $|\psi_{ak}\rangle \equiv V_q^k |\phi_{a0}\rangle$. According to Eq.(4), we may express the ground state $|\varphi_0\rangle$ and L low-lying states $|\varphi_k\rangle$, with $k = 1, \dots, L$ in terms of the q H-

orthogonal states $|\psi_k\rangle$ or $|\psi_{ak}\rangle$. In particular, the ground state $|\varphi_0\rangle$ takes the form: $|\varphi_0\rangle = \frac{1}{c_0} \sum_{k'=0}^{q-1} |\psi_{k'}\rangle$, which in turn allows us to expand it into a linear combination of the highly degenerate ground states. Therefore, the entanglement entropy $S(L, N)$ for the ground state $|\varphi_0\rangle$ may be evaluated. In fact, the ground state $|\varphi_0\rangle$ on the characteristic line $J_x/J_z = 0$ with $J_y/J_z > 0$ is highly entangled.

B. The ground state and the low-lying states from an exact diagonalization perspective

For the spin-1 ferromagnetic anisotropic biquadratic model (1) under PBCs, the ED simulations are performed for six chosen points $(J_x/J_z, J_y/J_z) = (0.35, 0.94), (0.3, 0.94), (0.2, 0.9), (0.2, 0.8), (0.15, 0.8)$ and $(0.1, 0.7)$ in the CF_x phase, and four chosen points $(J_x/J_z, J_y/J_z) = (0.25, 0.65), (0.3, 0.7), (0.35, 0.7)$ and $(0.4, 0.75)$ in the LL_{yz} phase, respectively.

We target at the ground state $|\varphi_0\rangle$ and the L low-lying states $|\varphi_k\rangle$ ($k = 1, \dots, L$), with the ground state energy E_0 and the energy eigenvalues E_k for each of the chosen points in the two phases. We take the point $(J_x/J_z = 0.2, J_y/J_z = 0.9)$ in the CF_x phase and the point $(J_x/J_z = 0.3, J_y/J_z = 0.7)$ in the LL_{yz} phase, with the system size $L = 4, 8$ and 16 , as two illustrative examples. The ground state energy per lattice site, denote as $e_0 \equiv E_0/L$, and the energy eigenvalues per lattice site, denote as $e_k \equiv E_k/L$, are listed in Table I and in Table II, respectively. The numerical results clearly show that the L low-lying states $|\varphi_k\rangle$ occur in pair, in addition to the non-degenerate ground state $|\varphi_0\rangle$ for even L 's. The same pattern shows up at the other five points in the CF_x phase and at the three other points in the LL_{yz} phase (but are not shown here).

Since the symmetry group $U(1) \times U(1)$ is not implemented during our numerical simulations, the L low-lying states $|\varphi_k\rangle$ ($k = 1, \dots, L$) are not eigenvectors of the $U(1)$ symmetry generator K_{yz} . Hence, it is necessary to take one additional step to ensure the symmetry group $U(1)$ generated from K_{yz} . For our purpose, we take advantage of the operator $V_q = \prod_j \exp(i2\pi K_{yz}^j/q)$, with $q = L + 1$, to introduce 2×2 matrix $M_{l,q-l}$ for each pair of $|\varphi_l\rangle$ and $|\varphi_{q-l}\rangle$ ($l = 1, \dots, L/2$):

$$M_{l,q-l} = \begin{pmatrix} \langle \varphi_l | V | \varphi_l \rangle & \langle \varphi_l | V | \varphi_{q-l} \rangle \\ \langle \varphi_{q-l} | V | \varphi_l \rangle & \langle \varphi_{q-l} | V | \varphi_{q-l} \rangle \end{pmatrix}. \quad (S1)$$

Then, the diagonalization of the matrix $M_{l,q-l}$ yields simultaneous eigenvectors of the model Hamiltonian (1) and V_q , which are listed in Table III. Here, we remark that $\langle \varphi_l | V | \varphi_{q-l} \rangle$, defined as the elements of V_q between the two degenerate low-lying states $|\varphi_l\rangle$ and $|\varphi_{q-l}\rangle$, are evaluated. From now on, we use the same notations to denote the L low-lying states $|\varphi_m\rangle$ that are simultaneous eigenvectors of the model Hamiltonian (1) and V_q .

Hence, we conclude that the l -th low-lying states $|\varphi_l\rangle$ is degenerate with $q - l$ -th low-lying states $|\varphi_{q-l}\rangle$, in both the CF_x phase and the LL_{yz} phase, i.e., $E_l = E_{q-l}$ ($l = 1, \dots, L/2$).

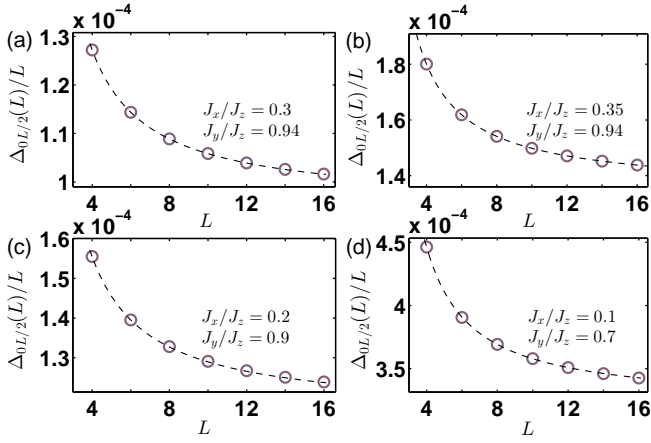


FIG. S1. (color online) The ratio $\Delta_{0L/2}(L)/L$ as a function of the system size L for four chosen points in the CF_x phase, with L ranging from 4 to 16.

Meanwhile, $|\varphi_l\rangle$ is mapped to $|\varphi_{q-l}\rangle$ and vice versa under the one-site translation operation, given PBCs are adopted.

We remark that the same pattern is not valid in the SPT_z phase. The ground state energy per lattice site $e_0(L)$ and the energy eigenvalues per lattice site, denoted as $e_k(L)$ ($k = 1, \dots, L$) are listed in Table IV, for the L low-lying states, at the point $(J_x/J_z = 0.4, J_y/J_z = 0.47)$ in the SPT_z phase. This makes it possible to distinguish the SPT_z phase from both the CF_x phase and the LL_{yz} phase.

In the CF_x phase and the LL_{yz} phase, the energy gaps $\Delta_{0L/2}(L)$, defined as $\Delta_{0L/2}(L) = E_{L/2}(L) - E_0(L)$, are scrutinized from an ED perspective, where $E_0(L)$ is the ground state energy per lattice site, and $E_{L/2}(L)$ is the energy eigenvalue per lattice site for the $L/2$ -th low-lying state.

In Fig. S1, we plot the ratio $\Delta_{0L/2}(L)/L$ as a function of the system size L for four chosen points: (a) $(J_x/J_z, J_y/J_z) = (0.3, 0.94)$, (b) $(J_x/J_z, J_y/J_z) = (0.35, 0.94)$, (c) $(J_x/J_z, J_y/J_z) = (0.2, 0.9)$, and (d) $(J_x/J_z, J_y/J_z) = (0.1, 0.7)$ in the CF_x phase. The ED simulations are performed for a few different values of the system size L , ranging from 4 to 16. According to Eq. (8), the energy gap $\Delta_{0L/2}(L)$ scales with the system size L as $\Delta_{0L/2}(L) = A \exp(\eta/L) + BL \exp(-\kappa L)$. Our simulation results for A and B , η and κ are listed in Table V. This amounts to performing an analysis of the finite-size corrections to the ground state energy E_0 for small L 's, accessible to the ED simulations. Although the results slightly deviate from those for larger L 's, they still indicate that $\Delta_{0L/2}(L)/L$ vanishes, as L gets large.

In Fig. S2, we plot the ratio $\Delta_{0L/2}(L)/L$ as a function of the system size L for four chosen points: (a) $(J_x/J_z, J_y/J_z) = (0.25, 0.65)$, (b) $(J_x/J_z, J_y/J_z) = (0.3, 0.7)$, (c) $(J_x/J_z, J_y/J_z) = (0.35, 0.7)$, and (d) $(J_x/J_z, J_y/J_z) = (0.4, 0.75)$ in the LL_{yz} phase. The energy gap $\Delta_{0L/2}(L)$ scales with the system size L as $\Delta_{0L/2}(L) \sim L$. Our simulation results indicate that $\Delta_{0L/2}(L)/L$ does not vanish, as L goes to ∞ .

We remark that the $L/2$ -th and $L/2 + 1$ -th low-lying states are degenerate, thus forming a pair, with the energy eigenvalue per lattice site, denoted as $e_{L/2}$, being equal to the maximum

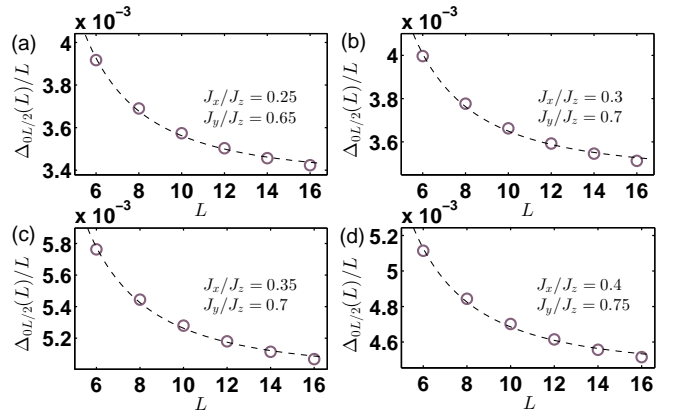


FIG. S2. (color online) The energy gap $\Delta_{0L/2}(L)$ as a function of the system size L for four chosen points in the LL_{yz} phase, with L ranging from 4 to 16.

J_x^2 among the L low-lying states $|\varphi_k\rangle$ ($k = 1, \dots, L$) in both the LL_{yz} phase and the CF_x phase. Actually, the two degenerate low-lying states are identified as $|\otimes_l \{0_y\}0_z\rangle_l$ and $|\otimes_l \{0_z\}0_y\rangle_l$ in the two phases. This observation offers compelling evidence for our conclusion that the ground state $|\varphi_0\rangle$ and L low-lying states $|\varphi_k\rangle$ ($k = 1, \dots, L$) are quasi-degenerate in the CF_x phase, but not in the LL_{yz} phase. In fact, the symmetry-broken ground states arise from an alternative SSB pattern for $U(1)$ that *only* occurs in the thermodynamic limit, with the ground state energy per lattice site being J_x^2 in the CF_x phase. Hence, they are (unentangled) factorized states such that the H-orthogonal states appear as a finite-size precursor to the symmetry-broken ground states. In contrast, this does not happen in the LL_{yz} phase, since the ground state energy per lattice site is not equal to J_x^2 . In other words, the ratio $\Delta_{0L/2}(L)/L$ vanishes in the CF_x phase, but it does not vanish in the LL_{yz} phase.

C. The entanglement entropy $S(L, N)$ in the SPT_z , LL_{yz} and CF_x phases

The entanglement entropy $S(L, N)$ is investigated to characterize the three distinct phases - the SPT_z , LL_{yz} and CF_x phases.

In Fig. S3, we plot the entanglement entropy $S(L, N)$, as a function of the block size N , for the three points $(J_x/J_z, J_y/J_z) = (0.2, 0.3)$, $(0.6, 0.65)$ and $(0.8, 0.82)$ in the SPT_z phase. It is found that the entanglement entropy $S(L, N)$ saturates, as the block size n increases. Here, the system size L is chosen to be $L = 60$. This indicates that an energy gap opens in this phase.

As for the LL_{yz} phase, we demonstrate that it is gapless and its low energy physics is described in terms of conformal field theory. To this end, we extract central charge c from a finite-size scaling analysis of the entanglement entropy $S(L, N)$. According to the conformal field theory [S4], $S(L, N)$ scales as

$$S(L, N) = \frac{c}{3} T(L, N) + S_0, \quad (S2)$$

TABLE I. The ground state energy per lattice site $e_0(L)$ and the energy eigenvalues per lattice site, denoted as $e_k(L)$ ($k = 1, \dots, L$), for the L low-lying states, respectively, with the system size $L = 4, 8$ and 16 , at the point ($J_x/J_z = 0.2, J_y/J_z = 0.9$) in the CF_x phase.

	$e_0(L)$	$e_1(L)$	$e_2(L)$	$e_3(L)$	$e_4(L)$	$e_5(L)$	$e_6(L)$	$e_7(L)$	$e_8(L)$
$L = 4$	0.03984448	0.03988474	0.03988474	0.04	0.04				
$L = 8$	0.03986720	0.03987561	0.03987561	0.03990076	0.03990076	0.03994237	0.03994237	0.04	0.04
$L = 16$	$e_0(L)$	$e_1(L)$	$e_2(L)$	$e_3(L)$	$e_4(L)$	$e_5(L)$	$e_6(L)$	$e_7(L)$	$e_8(L)$
	0.03987611	0.03987807	0.03987807	0.03988393	0.03988393	0.03989368	0.03989368	0.03990732	0.03990732
	$e_9(L)$	$e_{10}(L)$	$e_{11}(L)$	$e_{12}(L)$	$e_{13}(L)$	$e_{14}(L)$	$e_{15}(L)$	$e_{16}(L)$	
	0.03992480	0.03992480	0.03994610	0.03994610	0.03997119	0.03997119	0.04	0.04	

TABLE II. The ground state energy per lattice site $e_0(L)$ and the energy eigenvalues per lattice site, denoted as $e_k(L)$ ($k = 1, \dots, L$), for the L low-lying states, respectively, with the system size $L = 4, 8$ and 16 , at the point ($J_x/J_z = 0.3, J_y/J_z = 0.7$) in the LL_{yz} phase.

	$e_0(L)$	$e_1(L)$	$e_2(L)$	$e_3(L)$	$e_4(L)$	$e_5(L)$	$e_6(L)$	$e_7(L)$	$e_8(L)$
$L = 4$	0.08541595	0.08702758	0.08702758	0.09	0.09				
$L = 8$	0.08622324	0.08650791	0.08650791	0.08730797	0.08730797	0.08851379	0.08851379	0.09	0.09
$L = 16$	$e_0(L)$	$e_1(L)$	$e_2(L)$	$e_3(L)$	$e_4(L)$	$e_5(L)$	$e_6(L)$	$e_7(L)$	$e_8(L)$
	0.08648798	0.08655110	0.08655110	0.08673843	0.08673843	0.08704421	0.08704421	0.08745986	0.08745986
	$e_9(L)$	$e_{10}(L)$	$e_{11}(L)$	$e_{12}(L)$	$e_{13}(L)$	$e_{14}(L)$	$e_{15}(L)$	$e_{16}(L)$	
	0.08797491	0.08797491	0.08857788	0.08857788	0.08925689	0.08925689	0.09	0.09	

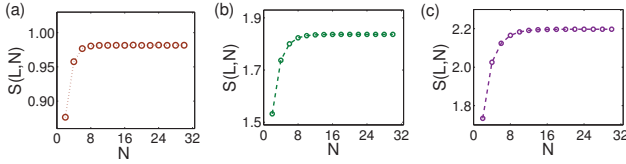


FIG. S3. (color online) The entanglement entropy $S(L, N)$, as a function of the block size N , for the three points $(J_x/J_z, J_y/J_z) =$ (a) $(0.2, 0.3)$, (b) $(0.6, 0.65)$ and (c) $(0.8, 0.82)$ in the SPT_z phase. Here, the system size L is 60.

with $T(L, N) = \log_2 [L/\pi \sin(\pi N/L)]$, where c is central charge, and S_0 is a (model-dependent) additive constant. For three chosen points $(J_x/J_z, J_y/J_z) = (0.45, 0.75)$, $(0.6, 0.75)$ and $(0.75, 0.85)$ in the LL_{yz} phase, we take advantage of the variational finite-size MPS algorithm [S5] to simulate the model (1) under PBCs. In Fig. S4, the entanglement entropy $S(L, N)$ versus $T(L, N)$, with the system size $L = 100$ and the bond dimension $\chi = 40$. In Table VII, we list our simulation results for central charge c , which are close to the exact value $c = 1$, with the relative errors less than 3%.

We turn to the CF_x phase. Actually, the ground state $|\varphi_0\rangle$ on the characteristic line $J_x/J_z = 0$ with $J_y/J_z > 0$ is highly entangled, in addition to highly entangled degenerate ground states on the characteristic line $J_y/J_z = 1$ with $J_x/J_z < 1$. Hence, one may anticipate that, even away from the two characteristic lines, the entanglement entropy $S(L, N)$ for a ground state in the CF_x phase must scale in a similar

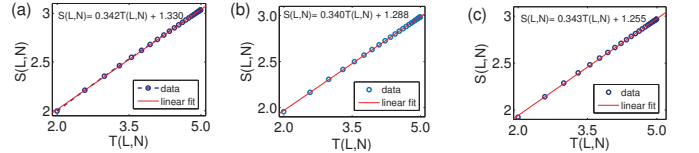


FIG. S4. The entanglement entropy $S(L, N)$ versus the block size $T(L, N)$ for three chosen points: (a) $(J_x/J_z, J_y/J_z) = (0.45, 0.75)$; (b) $(J_x/J_z, J_y/J_z) = (0.6, 0.75)$; (c) $(J_x/J_z, J_y/J_z) = (0.75, 0.85)$ in the LL_{yz} phase. Here, $L = 100$ and the bond dimension $\chi = 40$.

way. For a chosen point $(J_x/J_z, J_y/J_z) = (0.2, 0.9)$ in the CF_x phase, the model (1) is numerically simulated to yield the ground state wave function in the MPS representation by means of the variational finite-size MPS algorithm [S5]. In Fig. S5, the entanglement entropy $S(L, N)$, as a function of N for fixed L , is shown, with the system size $L = 30$ and the bond dimension $\chi = 25$. The entanglement entropy $S(L, N)$ does not saturate with increasing N until N reaches $L/2$, as expected. In addition, a finite-size scaling analysis is performed, with a universal finite-size scaling function $g(L, N)$ being $g(L, N) = N(1 - N/L)$ [S6]. As it turns out, the connection between the prefactor and the number of type-B GMs is lost.

TABLE III. The eigenvalues of the matrix $M_{l,q-l}$, defined as the elements of V_q between the two degenerate low-lying states $|\varphi_l\rangle$ and $|\varphi_{q-l}\rangle$, with the system size $L = 4, 8$ and 16 , at the point $(J_x/J_z = 0.2, J_y/J_z = 0.9)$ in the CF_x phase and at the point $(J_x/J_z = 0.3, J_y/J_z = 0.7)$ in the LL_{yz} phase.

	$l, q-l$ 1, L	$l, q-l$ 2, $L-1$	$l, q-l$ 3, $L-2$	$l, q-l$ 4, $L-3$	$l, q-l$ 5, $L-4$	$l, q-l$ 6, $L-5$	$l, q-l$ 7, $L-6$	$l, q-l$ 8, $L-7$
$L = 4$	$e^{i2\pi \times 1/(L+1)}$ $e^{i2\pi \times 4/(L+1)}$	$e^{i2\pi \times 2/(L+1)}$ $e^{i2\pi \times 3/(L+1)}$						
$L = 8$	$e^{i2\pi \times 1/(L+1)}$ $e^{i2\pi \times 8/(L+1)}$	$e^{i2\pi \times 2/(L+1)}$ $e^{i2\pi \times 7/(L+1)}$	$e^{i2\pi \times 3/(L+1)}$ $e^{i2\pi \times 6/(L+1)}$	$e^{i2\pi \times 4/(L+1)}$ $e^{i2\pi \times 5/(L+1)}$				
$L = 16$	$e^{i2\pi \times 1/(L+1)}$ $e^{i2\pi \times 16/(L+1)}$	$e^{i2\pi \times 2/(L+1)}$ $e^{i2\pi \times 15/(L+1)}$	$e^{i2\pi \times 3/(L+1)}$ $e^{i2\pi \times 14/(L+1)}$	$e^{i2\pi \times 4/(L+1)}$ $e^{i2\pi \times 13/(L+1)}$	$e^{i2\pi \times 5/(L+1)}$ $e^{i2\pi \times 12/(L+1)}$	$e^{i2\pi \times 6/(L+1)}$ $e^{i2\pi \times 11/(L+1)}$	$e^{i2\pi \times 7/(L+1)}$ $e^{i2\pi \times 10/(L+1)}$	$e^{i2\pi \times 8/(L+1)}$ $e^{i2\pi \times 9/(L+1)}$

TABLE IV. The ground state energy per lattice site $e_0(L)$ and the energy eigenvalues per lattice site, denoted as $e_k(L)$ ($k = 1, \dots, L$), for the L low-lying states, respectively, with the system size $L = 4, 8, 12$ and 16 , at the point $(J_x/J_z = 0.4, J_y/J_z = 0.47)$ in the SPT_z phase.

	$e_0(L)$	$e_1(L)$	$e_2(L)$	$e_3(L)$	$e_4(L)$	$e_5(L)$	$e_6(L)$	$e_7(L)$	$e_8(L)$
$L = 4$	0.11137607	0.13961933	0.13961933	0.16	0.16				
$L = 8$	0.11714763	0.12690821	0.12690821	0.13834780	0.13834780	0.14795967	0.14795967	0.14795967	0.14795967
$L = 12$	$e_0(L)$	$e_1(L)$	$e_2(L)$	$e_3(L)$	$e_4(L)$	$e_5(L)$	$e_6(L)$	$e_7(L)$	$e_8(L)$
	0.11775204	0.12379340	0.12379340	0.13087058	0.13087058	0.13184427	0.13184427	0.13184427	0.13184427
	$e_9(L)$	$e_{10}(L)$	$e_{11}(L)$	$e_{12}(L)$					
	0.13639967	0.13799444	0.13799444	0.13799444					
$L = 16$	$e_0(L)$	$e_1(L)$	$e_2(L)$	$e_3(L)$	$e_4(L)$	$e_5(L)$	$e_6(L)$	$e_7(L)$	$e_8(L)$
	0.11786452	0.12230268	0.12230268	0.12622999	0.12622999	0.12622999	0.12622999	0.12737090	0.12737090
	$e_9(L)$	$e_{10}(L)$	$e_{11}(L)$	$e_{12}(L)$	$e_{13}(L)$	$e_{14}(L)$	$e_{15}(L)$	$e_{16}(L)$	
	0.12962196	0.13069791	0.13069791	0.13100286	0.13100286	0.13100286	0.13100286	0.13271958	

TABLE V. The parameters A, B, η and κ are extracted from the energy gap $\Delta_{0L/2}(L) = A \exp(\eta/L) + B \exp(-\kappa L)$ for the model (1) under PBCs, with the system size L ranging from 4 to 16.

	$J_x/J_z = 0.3$	$J_x/J_z = 0.35$	$J_x/J_z = 0.2$	$J_x/J_z = 0.1$
	$J_y/J_z = 0.94$	$J_y/J_z = 0.94$	$J_y/J_z = 0.9$	$J_y/J_z = 0.7$
A	0.888×10^{-4}	1.212×10^{-4}	1.104×10^{-4}	2.767×10^{-4}
B	0.958×10^{-4}	1.362×10^{-4}	1.163×10^{-4}	3.234×10^{-4}
η	1.4	1.5	1.4	2.3
κ	0.821×10^{-4}	3.169×10^{-4}	0.609×10^{-4}	0.999×10^{-4}

TABLE VI. The parameters C and D are extracted from the ratio $\Delta_{0L/2}(L)/L$, for the model (1), with the system size L ranging from 6 to 16. Here, we assume that $\Delta_{0L/2}(L)/L = C + D/L^2$.

	$J_x/J_z = 0.25$	$J_x/J_z = 0.3$	$J_x/J_z = 0.35$	$J_x/J_z = 0.4$
	$J_y/J_z = 0.65$	$J_y/J_z = 0.7$	$J_y/J_z = 0.7$	$J_y/J_z = 0.75$
C	3.357×10^{-3}	3.448×10^{-3}	4.974×10^{-3}	4.437×10^{-3}
D	2.051×10^{-2}	2.012×10^{-2}	2.888×10^{-2}	2.485×10^{-2}

TABLE VII. Central charge c extracted from the entanglement entropy $S(L, N)$ versus $T(L, N)$ for three chosen points in the LL_{yz} phase. Our simulation results are close to the exact value $c = 1$, with the relative errors less than 3%.

$(J_x/J_z, J_y/J_z)$	(0.45, 0.75)	(0.6, 0.75)	(0.75, 0.85)
c	1.029	1.020	1.026

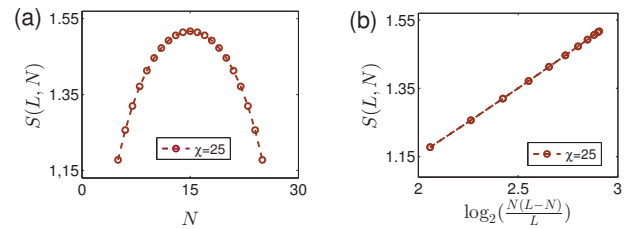


FIG. S5. (color online) The entanglement entropy $S(L, N)$ for the chosen point $(J_x/J_z, J_y/J_z) = (0.2, 0.9)$ in the CF_x phase, with the system size L being 30: (a) the entanglement entropy $S(L, N)$ versus the block size N ; (b) the entanglement entropy $S(L, N)$ versus the finite-size universal scaling function $\log_2(N(L-N)/L)$. Here, N ranges from 6 to 24, and the bond dimension χ is chosen to be $\chi = 25$.

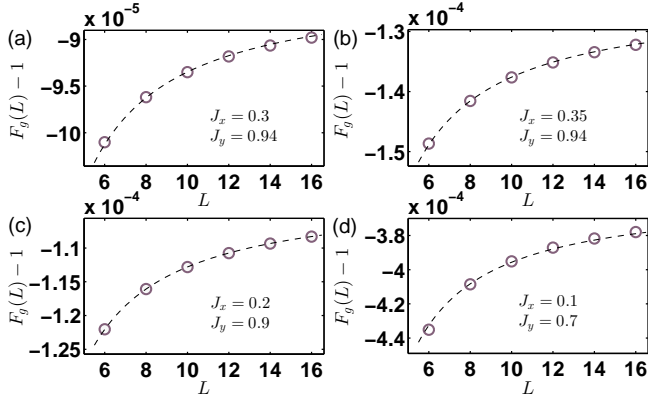


FIG. S6. (color online) The geometric average $F_g(L)$ of $F_{ll+1}(L) = |\langle \varphi_0 | P_{ll+1} | \varphi_0 \rangle|$ ($l = 1, \dots, L/2 - 1$), as a function of the system size L for the four chosen points: (a) $(J_x/J_z, J_y/J_z) = (0.3, 0.94)$, (b) $(J_x/J_z, J_y/J_z) = (0.35, 0.94)$, (c) $(J_x/J_z, J_y/J_z) = (0.2, 0.9)$, and (d) $(J_x/J_z, J_y/J_z) = (0.1, 0.7)$ in the CF_x phase, with P_{ll+1} representing the exchange operations acting on the two nearest-neighbor unit cells l and $l+1$ ($l = 1, \dots, L/2 - 1$), and the system size L ranging from 6 to 16.

TABLE VIII. The parameter R is extracted from the geometric average $F_g(L) = 1 - R(A \exp(\eta/L)/L + B \exp(-\kappa L))$ for four chosen points: (a) $(J_x/J_z, J_y/J_z) = (0.3, 0.94)$, (b) $(J_x/J_z, J_y/J_z) = (0.35, 0.94)$, (c) $(J_x/J_z, J_y/J_z) = (0.2, 0.9)$, and (d) $(J_x/J_z, J_y/J_z) = (0.1, 0.7)$ in the CF_x phase, with the system size L ranging from 6 to 16. Here, A , B , η and κ are taken from Table IX, extracted from the finite-size corrections to the ground state energy per lattice site, $e_0(L)$.

	$J_x/J_z = 0.3$	$J_x/J_z = 0.35$	$J_x/J_z = 0.2$	$J_x/J_z = 0.1$
	$J_y/J_z = 0.94$	$J_y/J_z = 0.94$	$J_y/J_z = 0.9$	$J_y/J_z = 0.7$
R	0.885	0.919	0.875	1.107

D. Emergent permutation symmetry group $S_{L/2}$ in the CF_x phase

In the CF_x phase, an approximate permutation symmetry group $S_{L/2}$ emerges that becomes *exact* in the thermodynamic limit.

For our purpose, we have to evaluate the fidelity $F(L)$, which essentially compares the ground state $|\varphi_0\rangle$ with the state $P|\varphi_0\rangle$, resulted from the action of a permutation operation P on $|\varphi_0\rangle$. Mathematically, the permutation group $S_{L/2}$ is generated from $L/2 - 1$ generators P_{ll+1} , representing the exchange operations acting on the two nearest-neighbor unit cells l and $l+1$ ($l = 1, \dots, L/2 - 1$). As a result, we have $F_{ll+1}(L) = |\langle \varphi_0 | P_{ll+1} | \varphi_0 \rangle|$ ($l = 1, \dots, L/2 - 1$).

Hence, we need to introduce the geometric average of $F_{ll+1}(L)$, denoted as $F_g(L)$, as a measure to quantify the extent to which the approximate permutation symmetry $S_{L/2}$ for finite L 's deviates from the exact one:

$$F_g(L) = \sqrt[L/2-1]{\prod_{l=1}^{L/2-1} F_{ll+1}(L)}. \quad (\text{S3})$$

The presence of the approximate permutation symmetry $S_{L/2}$ implies that any two-point correlation function does not depend on the distance between the two points, up to $1/L'$, with r being a positive integer. Since this statement works for the Hamiltonian density in (1) and P_{ll+1} , one may conclude that the ground state energy per lattice site approaches J_x^2 , in exactly the same way as $F_g(L)$ approaches 1. In other words, $e_0(L) - J_x^2$ should be proportional to $F_g(L) - 1$. Equivalently, $F_g(L)$ scales as

$$F_g(L) = 1 - R \left(\frac{Ae^{\eta/L}}{L} + Be^{-\kappa L} \right), \quad (\text{S4})$$

where R is a positive constant.

In Fig. S6, we plot $F_g(L) - 1$ versus L for four chosen points: (a) $(J_x/J_z, J_y/J_z) = (0.3, 0.94)$, (b) $(J_x/J_z, J_y/J_z) = (0.35, 0.94)$, (c) $(J_x/J_z, J_y/J_z) = (0.2, 0.9)$, and (d) $(J_x/J_z, J_y/J_z) = (0.1, 0.7)$ in the CF_x phase, when A , B , η and κ are taken from Table IX, extracted from the finite-size corrections to the ground state energy per lattice site, $e_0(L)$. The best fit is performed to yield the parameter R , as listed in Table VIII.

E. Finite-size corrections to the ground state energy E_0 : the energy expectation value \bar{E} for a H-orthogonal state

On the characteristic line $J_x = 0$ with $J_y/J_z > 0$, a factorized ground state takes the form $|\phi_f(L)\rangle = \bigotimes_l |v_1 v_2\rangle_l$ [S3], where $|v_1 v_2\rangle_l = |v_1\rangle_{2l-1} |v_2\rangle_{2l}$, with $|v_1\rangle_{2l-1}$ and $|v_2\rangle_{2l}$ being a vector in a local spin space at the two nearest-neighbor lattice sites $2l-1$ and $2l$ ($l = 1, \dots, L/2$), respectively. They take the form

$$|v_1\rangle_{2l-1} = \sin \zeta |0_y\rangle_{2l-1} + e^{i\theta} \cos \zeta |0_z\rangle_{2l-1}, \quad (\text{S5})$$

$$|v_2\rangle_{2l} = \frac{J_y \cos \zeta}{\sqrt{J_y^2 \cos^2 \zeta + J_z^2 \sin^2 \zeta}} |0_y\rangle_{2l} + e^{-i\theta} \frac{J_z \sin \zeta}{\sqrt{J_y^2 \cos^2 \zeta + J_z^2 \sin^2 \zeta}} |0_z\rangle_{2l},$$

where ζ and θ are two free parameters that are real, and $|0_y\rangle_{2l-1/2l}$ and $|0_z\rangle_{2l-1/2l}$ are basis states, with an eigenvalue being zero, for the spin operators $S_{2l-1/2l}^y$ and $S_{2l-1/2l}^z$, respectively. Here, we have introduced L as an argument in a wave function to indicate the dependence on L .

We stress that $|\phi_f(L)\rangle$ constitute a two-parameter family of ground states on the characteristic line $J_x = 0$ with $J_y/J_z > 0$. However, only $q = L + 1$ states among them are linearly independent to each other. A convenient way to take advantage of this fact is to exploit V_q and $|\phi_0(L)\rangle$, already defined in the main text, to introduce q H-orthogonal states $|\psi_k\rangle$ on the characteristic line $J_x = 0$ with $J_y/J_z > 0$: $|\psi_k(L)\rangle \equiv (V_q)^k |\phi_0(L)\rangle$ [S7] ($k = 0, 1, \dots, L$). Hence, it is the cyclic group Z_q that connects the q H-orthogonal states $|\psi_k(L)\rangle$, which becomes $U(1)$ in the thermodynamic limit. For convenience, the explicit expression for $|\phi_0(L)\rangle$ is cited: $|\phi_0\rangle = \bigotimes_j |v\rangle_j$, where $|v\rangle_j = \mu |0_y\rangle_j + \nu |0_z\rangle_j$, with $\mu^2 + \nu^2 = 1$ and $\mu = \sqrt{J_y/(J_y + J_z)}$.

It is plausible to assume that, away from the characteristic line $J_x = 0$ with $J_y/J_z > 0$ in the CF_x phase, for a fixed value of J_y , the q H-orthogonal states $|\psi_k\rangle$ may be expanded into

an asymptotic series, with a leading term being proportional to $(V_q)^k |\phi_0(L)\rangle$. For our purpose, we focus on $|\psi_0(L)\rangle$, which takes the form

$$|\psi_0(L)\rangle = \frac{1}{\sqrt{N_0}} \sum_n \omega_n |\phi(L, n)\rangle, \quad (\text{S6})$$

where $|\phi(L, n)\rangle$ denote a set of orthonormal states: $\langle \phi(L, m) | \phi(L, n) \rangle = \delta_{mn}$, and ω_n ($n = 0, 1, \dots$) denote the coefficients in $|\phi(L, n)\rangle$, with $N_0 = \sum_j |\omega_j|^2$. Without loss of generalities, one may assume that ω_0 is a positive number. In particular, we set $|\phi(L, 0)\rangle = |\phi_0(L)\rangle$, which is permutation-invariant with respect to the unit cells consisting of the two nearest-neighbor lattice sites.

Our aim is to determine $|\psi_0(L)\rangle$ up to the first order correction. This amounts to determining $|\phi(L, 1)\rangle$, which may be achieved if we act the Hamiltonian \mathcal{H} , as presented in Eq.(1), on $|\phi(L, 0)\rangle$ successively. As a result, we have

$$\begin{aligned} \mathcal{H}|\phi(L, 0)\rangle &= J_x^2 L |\phi(L, 0)\rangle + a \sqrt{L} |\phi(L, 1)\rangle, \\ \mathcal{H}|\phi(L, 1)\rangle &\simeq a \sqrt{L} |\phi(L, 0)\rangle + J_x^2 L \left(1 - \frac{b}{L}\right) |\phi(L, 1)\rangle, \end{aligned}$$

where $a = J_x(J_z - J_y)$ and $b = 3$. Note that a is a positive number in the LL phases. Here, $|\phi(L, 1)\rangle$, orthogonal to $|\phi(L, 0)\rangle$, takes the form

$$|\phi(L, 1)\rangle = \frac{1}{\sqrt{C_{L/2}^1}} \sum_P |\underbrace{v v \dots v v}_{L/2-1} \underbrace{|0_x 0_x\rangle}_1\rangle, \quad (\text{S7})$$

where the sum is taken over all the permutations P for a given partition, with $L/2 - 1$ and 1 denoting the numbers of the unit cells in $|v v\rangle$ and $|0_x 0_x\rangle$, respectively. If we choose $\omega_1 = u / \sqrt{L}$, with u being a real number to be determined, then N_0 takes the form

$$N_0 \approx \sqrt{\omega_0^2 + \omega_1^2} = \sqrt{\omega_0^2 + |u|^2/L}. \quad (\text{S8})$$

Now we are ready to evaluate the energy expectation value $\bar{E}(L)$ for a H-orthogonal state, which takes the form

$$\bar{E}(L) = J_x^2 L - \frac{2|u|a}{\omega_0} + O\left(\frac{1}{L}\right). \quad (\text{S9})$$

Here, we have chosen u to be negative to ensure that $\bar{E}(L)$ is less than $J_x^2 L$. As follows from the Cauchy-Schwarz inequality: $|u|a \leq (|u|^2 + a^2)/2$, we have

$$\bar{E}(L) \geq J_x^2 L - \frac{|u|^2 + a^2}{\omega_0} + O\left(\frac{1}{L}\right), \quad (\text{S10})$$

where the equality is valid if $|u| = a$. In other words, it is necessary to choose $|u| = a$, in order to satisfy the physical requirement that the ground state energy $E_0(L)$ must be as low as possible, given the relation between $\bar{E}(L)$ and $E_0(L)$ in Eq.(6). Hence, we have

$$\bar{E}(L) = J_x^2 L - \frac{2a^2}{\omega_0} + O\left(\frac{1}{L}\right). \quad (\text{S11})$$

If we proceed to the next order in the asymptotic series in Eq. (S6), it is possible to figure out the sub-leading correction $-g/L$, with g being a constant. Instead, we restrict ourselves to pointing out that g must be positive. Physically, this is due to the fact that a ground state yields the lowest energy expectation value. Indeed, if g were negative, then it would yield a higher energy expectation value. If so, we should have stopped to proceed in the first place. In other words, the asymptotic series in Eq. (S6) would terminate, but obviously that is not the case. In fact, we attempt to approximate the ground state $|\varphi_0\rangle$ and the L low-lying states $|\varphi_k\rangle$ ($k = 1, \dots, L$) in terms of q permutation-invariant H-orthogonal states, as seen from Eq.(S6). However, the permutation symmetry group $\mathcal{S}_{L/2}$ is approximate for finite L 's, but becomes exact when L tends to infinity. Hence, we have $\bar{E}(L) = J_x^2 L - \frac{2a^2}{\omega_0} - \frac{g}{L}$, with g being positive, which may be rewritten as follows

$$\bar{E}(L) \approx J_x^2 L - A e^{\eta/L}, \quad (\text{S12})$$

where $A = 2a^2/\omega_0$ and $\eta = \omega_0 g/(2a^2)$. Substituting into Eq.(6), we are led to the finite-size corrections to the ground state energy $E_0(L)$ in Eq.(8).

Our construction above shows that the ground state and the low-lying states are very close to each other, which explains why it is challenging to simulate the spin-1 ferromagnetic anisotropic biquadratic model (1) [S3] in the CF_x phase by means of the tensor network algorithms [S8, S9]. Therefore, it becomes important to look into the model from an ED perspective.

A few remarks are in order. First, the second term in Eq.(S10) originates from the emergent permutation symmetry in the ground state subspace and the third term in Eq.(S10) originates from an alternative SSB pattern for $\text{U}(1)$. Both of them vanish when the thermodynamic limit is approached. Second, it is the finite-size corrections to the ground state energy that mark an essential difference between the CF_x phase and the LL_{yz} phase. The former is scale-invariant, but not conformally invariant, whereas the latter is conformally invariant, with central charge being one, subject to the finite-size corrections to the ground state energy predicted from conformal field theory [S10, S11]. Third, our asymptotic analysis suggests that the q -orthogonal states $|\psi_k\rangle$, up to the first-order correction, are permutation-invariant, and the finite-size corrections to the ground state energy takes the same form as that from a heuristic argument for generic permutation-invariant states.

F. Finite-size correlations to the ground state energy per lattice site $e_0(L)$ from the finite-size DMRG simulations

The ground state energy per lattice site, denoted as $e_0(L)$, is evaluated from the finite-size DMRG simulations [S12, S13] for the model Hamiltonian (1) under PBCs. The finite-size corrections to the ground state energy per lattice site, $e_0(L)$, take the form

$$e_0(L) = J_x^2 - A \frac{e^{\eta/L}}{L} - B e^{-\kappa L}. \quad (\text{S13})$$

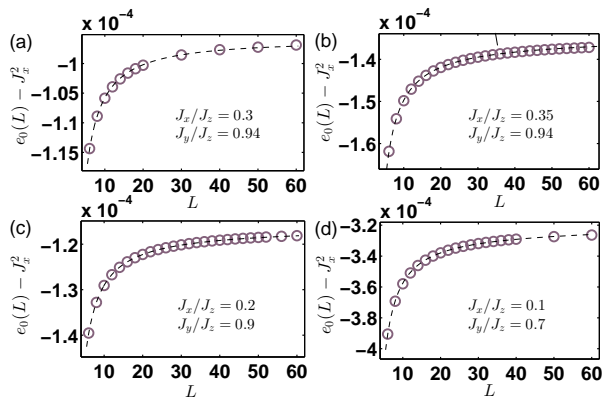


FIG. S7. (color online) The finite-size corrections to the ground state energy per lattice site, denoted as $e_0(L)$, for four chosen points: (a) $(J_x/J_z, J_y/J_z) = (0.3, 0.94)$, (b) $(J_x/J_z, J_y/J_z) = (0.35, 0.94)$, (c) $(J_x/J_z, J_y/J_z) = (0.2, 0.9)$, and (d) $(J_x/J_z, J_y/J_z) = (0.1, 0.7)$ in the CF_x phase. Here, the finite-size DMRG algorithm is exploited to simulate the model (1) under PBCs, with the system size L ranging from 6 to 60.

TABLE IX. The parameters A , B , η and κ are extracted from the finite-size corrections to the ground state energy per lattice site, denoted as $e_0(L)$, for the model (1), with the system size L ranging from 6 to 60.

	$J_x/J_z = 0.3$	$J_x/J_z = 0.35$	$J_x/J_z = 0.2$	$J_x/J_z = 0.1$
	$J_y/J_z = 0.94$	$J_y/J_z = 0.94$	$J_y/J_z = 0.9$	$J_y/J_z = 0.7$
A	0.919×10^{-4}	1.221×10^{-4}	1.079×10^{-4}	2.735×10^{-4}
B	0.952×10^{-4}	1.355×10^{-4}	1.165×10^{-4}	3.231×10^{-4}
η	1.4	1.6	1.5	2.4
κ	0.580×10^{-4}	0.645×10^{-4}	0.303×10^{-4}	0.976×10^{-4}

Indeed, the second term originates from the emergent permutation symmetry in the ground state subspace, which in turn is relevant to a gapped GM when the symmetry group $SU(2) \times U(1)$ on the characteristic line $J_y = J_z$ is explicitly bro-

ken to $U(1) \times U(1)$, away from the characteristic line $J_y = J_z$. Meanwhile, the third term originates from an alternative SSB pattern for $U(1)$. The finite-size corrections to the ground state energy mark an essential difference between the CF phases and the LL phases. Here, we emphasize that the presence of $\exp(\eta/L)$ in the second term represents the emergence of a length scale, in addition to another length scale arising from Z_q in the third term. Therefore, two length scales are involved, competing with each other, in the CF_x phase.

In the main text, we have performed the best fit for the ground state energy per lattice site, $e_0(L)$ against the theoretical prediction in Eq.(S13). Here, the best fit is performed for other four chosen points deep inside the CF_x phase. In Fig. S7, we plot $e_0(L)$ versus L for the four chosen points. Our simulation results for A and B , η and κ are listed in Table IX. As we have seen, A and B vanish, as J_x/J_z gets close to 0 and J_y/J_z gets close to 1, since no finite-size corrections arise on the two characteristic lines $J_x/J_z = 0$ and $J_y/J_z = 1$.

Note that the finite-size corrections to the ground state energy per lattice site, $e_0(L)$, are always negative, in the CF_x phase (also cf. Ref. [S3]), thus implying that the ground state energy per lattice site, $e_0(L)$, approaches J_x^2 from below, as L tends to infinity. Hence, as follows from the q H-orthogonal states, the symmetry group $U(1)$, viewed as a limit of Z_q as $q \rightarrow \infty$, is spontaneously broken in the thermodynamic limit. As a consequence, no gapless GM emerges, thus leading to an alternative SSB pattern for $U(1)$. The apparent contradiction with the Goldstone theorem [S14–S16] requires clarification of the semantic meaning for continuous SSB. That is, the dichotomy between continuous symmetry groups and discrete symmetry groups is not necessarily identical to that between continuous SSB and discrete SSB.

G. Acknowledgements

We are grateful to Murray Batchelor, John Fjaerestad and Ian McCulloch for comments and suggestions to improve the manuscript.

- [S1] Q.-Q. Shi, Y.-W. Dai, H.-Q. Zhou, and I. McCulloch, arXiv: 2201.01071 (2022).
- [S2] H.-Q. Zhou, Q.-Q. Shi, I. P. McCulloch, and M. T. Batchelor, arXiv: 2302.13126 (2023).
- [S3] Q.-Q. Shi, Y.-W. Dai, S.-H. Li, and H.-Q. Zhou, arXiv: 2204.05692 (2022).
- [S4] P. Calabrese and J. Cardy, J. Stat. Mech. P06002 (2004).
- [S5] F. Verstraete, D. Porras, and J. I. Cirac, Phys. Rev. Lett. **93**, 227205 (2004).
- [S6] H.-Q. Zhou, Q.-Q. Shi, I. P. McCulloch, and M. T. Batchelor, arXiv: 2304.11339 (2023).
- [S7] Q.-Q. Shi, H.-Q. Zhou, and M. T. Batchelor, Sci. Rep. **5**, 7673 (2015).
- [S8] G. Vidal, Phys. Rev. Lett. **98**, 070201 (2007).
- [S9] F. Verstraete, D. Porras, and J. I. Cirac, Phys. Rev. Lett. **93**, 227205 (2004).
- [S10] H. W. J. Blöte, J. Cardy, and M. P. Nightingale, Phys. Rev. Lett. **56** 742 (1986).
- [S11] I. Affleck, Phys. Rev. Lett. **56** 746 (1986).
- [S12] S. R. White, Phys. Rev. Lett. **69**, 2863 (1992).
- [S13] S. R. White, Phys. Rev. B, **48**, 345 (1993).
- [S14] J. Goldstone, Nuovo Cimento **19**, 154 (1961).
- [S15] J. Goldstone, A. Salam, and S. Weinberg, Phys. Rev. **127**, 965 (1962).
- [S16] Y. Nambu and G. Jona-Lasinio, Phys. Rev. **122**, 345 (1961).